Infrared features of the Landau gauge QCD

Sadataka Furui*
School of Science and Engineering, Teikyo University, 320-8551, Japan

Hideo Nakajima†
Department of Information Science, Utsunomiya University, 321-8585, Japan

(Received 12 May 2003; revised manuscript received 29 October 2003; published 28 April 2004)

The infrared features of Landau gauge QCD are studied by lattice simulation of $\beta=6.0,16^4,24^4,32^4$ and $\beta=6.4,32^4,48^4$. We adopt two definitions of the gauge field, (1) U linear and (2) log$U$, and measured the gluon propagator and ghost propagator. The infrared singularity of the gluon propagator is less than that of the tree level result, but the gluon propagator at 0 momentum remains finite. The infrared singularity of the ghost propagator is stronger than the tree level. The QCD running coupling measured by using the gluon propagator and the ghost propagator has a maximum $\alpha_s(p)\simeq 1$ at around $p=0.5$ GeV and decreases as p approaches 0. The data are analyzed with use of the formula of the principle of minimal sensitivity and the effective charge method, and by the contour-improved perturbation method, which suggest the necessity of the resummation of the perturbation series in the infrared region together with the existence of the infrared fixed point. The Kugo-Ojima parameter is about -0.8 in contrast with the theoretically expected value of -1. The color off-diagonal part of the ghost propagator in the Landau gauge is consistent with zero, and its fluctuation can be parametrized as a constant/$(qa)^4$.

DOI: 10.1103/PhysRevD.69.074505 PACS number(s): 12.38.Gc, 11.15.Ha, 11.15.Tk

I. INTRODUCTION

Two decades ago, Kugo and Ojima proposed a criterion for the absence of colored massless asymptoptic states in Landau gauge QCD using the Beecchi-Rouet-Stora-Tyutin (BRST) symmetry [1]. They suggested to measure the two-point function of the covariant derivative of the ghost and the commutator of the antighost and gauge field:

$$\left(\delta_{\mu\nu}-\frac{q_\mu q_\nu}{q^2}\right)u^{ab}(q^2) = \frac{1}{V}\sum_{x,y} e^{-ip(x-y)}\left\langle \mathrm{tr}\left(\lambda^{a\dagger}D_\mu\frac{1}{-\partial D}[A_\nu,\lambda^b]\right)_{xy}\right\rangle. \quad (1)$$

They showed that $u^{ab}(0)=\delta^{ab}u(0)$ satisfies

$$1+u(0)=\frac{Z_1}{Z_3}=\frac{1}{\tilde{Z}_3}, \quad (2)$$

where Z_3 is the gluon wave function renormalization factor, Z_1 is the gluon vertex renormalization factor, and $\tilde{Z}_3$ is the ghost wave function renormalization factor, respectively. Kugo claimed that confinement is realized either by (1) $Z_1=0$ and $Z_3=$ finite or (2) $Z_1/Z_3=0$ but (and) $Z_3=0$. The divergence of $\tilde{Z}_3$ implies $u(0)=-1$ and the presence of a long-range correlation between colored sources.

As shown by Gribov [2], the Landau gauge is not unique and the uniqueness of the gauge field can be achieved via restriction to the fundamental modular region (FMR)—i.e., the region where the norm is the absolute minimum [3,4]. We adopted the smearing gauge fixing [5] to make the configuration close to the FMR. We observed the proximity of the gauge configurations with and without smearing gauge fixing, but the overlap of the Gribov region and FMR remains to be investigated.

The confinement scenario was recently reviewed in the framework of the renormalization group equation and dispersion relation [6]. It was shown that the gluon dressing function $Z_A(q^2)$ defined from the gluon propagator of SU(n),

$$D_{\mu\nu}(q)=\frac{1}{n^2-1}\sum_{x=\mathbf{x},t} e^{-ikx}\,\mathrm{Tr}\langle A_\mu(x)^\dagger A_\nu(0)\rangle = \left(\delta_{\mu\nu}-\frac{q_\mu q_\nu}{q^2}\right)D_A(q^2), \quad (3)$$

as $Z_A(q^2)=q^2D_A(q^2)$, satisfies the superconvergence relation, and the gluon dressing function at zero momentum does not necessarily vanish as Gribov and Zwanziger conjectured, but it could be finite. A systematic study of lattice data indeed establishes the infrared finiteness of the gluon propagator [7].

The ghost propagator is defined as the Fourier transform of an expectation value of the inverse Faddeev-Popov (FP) operator $\mathcal{M}$:

$$D_G^{ab}(x,y)=\langle \mathrm{tr}\langle \lambda^a x|(\mathcal{M}[U])^{-1}|\lambda^b y\rangle\rangle, \quad (4)$$

where the outmost $\langle\cdots\rangle$ denotes average over samples U. The infrared behavior of the ghost propagator in the renormalization group approach depends on the gauge, and whether it satisfies the superconvergence relation is not clear. In maximal Abelian gauge, it is conjectured that the off-

*Electronic address: furui@umb.teikyo-u.ac.jp; URL http://albert.umb.teikyo-u.ac.jp/furui_lab/furuipbs.htm
†Electronic address: nakajima@is.utsunomiya-u.ac.jp

diagonal gluon and off-diagonal ghost satisfy the superconvergence relation, but the diagonal ghost does not, and it is the source of the long-range correlation. We remark that Nishijima proposed a sufficient condition for the confinement as $Z_3=0$, based on the convergence of the spectral function [8].

The nonperturbative color confinement mechanism was studied with the Dyson-Schwinger approach [9] and lattice simulation [10–16]. We produced SU(3) gauge configurations by using the heat-bath method [17,18] and performed gauge fixing [13]. We analyzed lattice Landau gauge configurations of $\beta=6.0$, 16^4, 24^4, 32^4 and $\beta=6.4$, 32^4, 48^4 produced at KEK. Progress reports are presented in [13] and an extensive report will be published elsewhere. The gauge field is defined from the link variables as

$$\log U \text{ type: } U_{x,\mu}=e^{A_{x,\mu}},\ A^{\dagger}_{x,\mu}=-A_{x,\mu},$$

$$U\text{-linear type: } A_{x,\mu}=\frac{1}{2}(U_{x,\mu}-U^{\dagger}_{x,\mu})|_{trless\ p.}$$

The fundamental modular region of lattice size L is specified by the global minimum along the gauge orbits—i.e.,

$$\Lambda_L=\{U|F_U(1)=\mathrm{Min}_g F_U(g)\},\ \Lambda_L\subset\Omega_L,$$

where Ω_L is called the Gribov region (local minima) and $\Omega_L=\{U|-\partial D(U)\geqslant 0,\ \partial A(U)=0\}$.

Here $F_U(g)$ for the two options are [19,20]

$$F_U(g)=||A^g||^2=\Sigma_{x,\mu}\mathrm{tr}(A^{g\dagger}{}_{x,\mu}A^g_{x,\mu}),$$
$$F_U(g)=\Sigma_{x,\mu}(1-\tfrac{1}{3}\mathrm{Re\ tr}U^g_{x,\mu}),$$

respectively.

The Landau gauge fixing in the log$U$ type is performed by Newton's method where the linear equation is solved up to third order of the gauge field, and then the Poisson equation is solved by the Green's function method for 16^4,24^4 lattices and by the multigrid method for 32^4,48^4 lattices [13]. The gauge fixing in the U-linear type is performed by the standard overrelaxation method. The accuracy of $\partial A(U)=0$ is 10^{-4} in the maximum norm.

In the calculation of the ghost propagator—i.e., inverse FP operator—we adopt the perturbative method with use of the multigrid Poisson solver [21], whose accuracy was kept within 10^{-5}, and we set 1% as an ending condition in the method [13]. But later we also introduce the straightforward and preconditioned conjugate gradient (CG) methods [22] for cross-checking of the calculation. In the preconditioned CG method, we take for the preconditioning operation the same truncated perturbation series of inversion as that of the perturbative method. In the CG method, the accuracy of the convergence of the series is set to be less than 5% in the L_2 norm.

We analyze these data using a method inspired by the principle of minimal sensitivity (PMS) and/or the effective charge method [23,24] and the contour-improved perturbation method [25].

In Sec. II we explain the method of analysis, and in Sec. III the lattice data are presented and compared with results of the theoretical analysis. We performed a cross-check of our program of SU(3) by performing the SU(2) lattice simulation. In Sec. IV we show our data and compare with those results of other groups. Our conclusion and outlook are presented in Sec. V. Some details of our method of calculating the FP inverse operator are given in the Appendix.

II. METHOD OF ANALYSIS

In the infrared region, the QCD perturbation series does not converge and truncation of the renormalization group equation and resummation of the series to evaluate the renormalon effect was proposed [26]. On the other hand, the possibility of the presence of an infrared fixed point was discussed and methods to bridge infrared and ultraviolet regions via the renormalization group equation were proposed [23,24]. The method was recently applied to an analysis of lattice data [27] and succeeded in explaining qualitatively the data. We briefly review the method.

A. PMS and the effective charge method

In the PMS method, the nth-order approximation to the physical quantity $\mathcal{R}$ is expressed by the corresponding series of coupling constant $h^{(n)}$ which is defined as a solution of

$$\beta_0\log\frac{\mu^2}{\Lambda^2}=\frac{1}{h}+\frac{\beta_1}{\beta_0}\log(\beta_0 h)+\int_0^h dx\left(\frac{1}{x^2}-\frac{\beta_1}{\beta_0 x}-\frac{\beta_0}{\beta_0 x^2+\beta_1 x^3+\cdots+\beta_n x^{n+2}}\right), \quad (5)$$

where the scheme-independent constant and logarithmic term are separated.

When $\mathcal{R}$ is the QCD running coupling from the triple gluon vertex from up to three-loop diagrams in the modified minimal subtraction ($\overline{\mathrm{MS}}$) scheme, one sets the scale μ^2 equal to the external scale q^2 and expresses

$$\mathcal{R}^n=h^{(n)}(1+A_1h^{(n)}+A_2h^{(n)2}+\cdots+A_nh^{(n)n}), \quad (6)$$

where in the case of $n=3$, $A_1=70/3$, $A_2=\frac{516217}{576}-\zeta_3\frac{153}{4}$, $A_3=\frac{304676635}{6912}-\zeta_3\frac{299961}{64}-\zeta_5\frac{81825}{64}$ [28].

When one defines $y_{\overline{\mathrm{MS}}}(q)$ as a solution of

$$1/y_{\overline{\mathrm{MS}}}(q)=\beta_0\log(q/\Lambda_{\overline{\mathrm{MS}}})^2-\frac{\beta_1}{\beta_0}\log[\beta_0 y_{\overline{\mathrm{MS}}}(q)] \quad (7)$$

and expresses the solution of Eq. (5),

$$h(q)=y_{\overline{\mathrm{MS}}}(q)\left\{1+y_{\overline{\mathrm{MS}}}(q)^2[\overline{\beta}_2/\beta_0-(\beta_1/\beta_0)^2]+y_{\overline{\mathrm{MS}}}(q)^3\frac{1}{2}[\overline{\beta}_3/\beta_0-(\beta_1/\beta_0)^3]+\cdots\right\}, \quad (8)$$

where $\beta_0=11$, $\beta_1=102$, $\overline{\beta}_2=\frac{2857}{2}$, $\overline{\beta}_3=\frac{149753}{6}+3564\zeta_3$, we can calculate $\mathcal{R}$ via Eq. (6).

The parameter $y_{\overline{\rm MS}}(q)$ can be expressed as y defined as a solution of

$$\beta_0 \log\frac{\mu^2}{\Lambda^2} = \frac{1}{y} + \frac{\beta_1}{\beta_0}\log(\beta_0 y) \tag{9}$$

and the function

$$k(q^2,y) = \frac{1}{y} + \frac{\beta_1}{\beta_0}\log(\beta_0 y) - \beta_0 \log(q^2/\Lambda^2_{\overline{\rm MS}}). \tag{10}$$

In [27] the parameter y is fixed via minimization of $|(\mathcal{R}^n(y)-\mathcal{R}^1(y))/\mathcal{R}^1(y)|$ for each q^2. There are subtle problems in fixing y of PMS in the low-energy region [29]. We leave the fitting of the low-energy region for the future and we fix y at $\mu=1.97$ GeV by solving

$$1/y = \beta_0 \log(\mu/\Lambda)^2 - \frac{\beta_1}{\beta_0}\log(\beta_0 y). \tag{11}$$

The choice of $\mu=1.97$ GeV corresponds to the inverse lattice unit $1/a$ of $\beta=6.0$ and chosen by [11] as the factorization scale of the effective charge method. When $\Lambda=\Lambda_{\overline{\rm MS}}=0.237$ GeV we find the solution $y=0.01594$, and we call this method of choosing y at a specific μ and define α_s from ghost-ghost-gluon coupling, the $\widetilde{\rm MOM}$ scheme.

B. Contour-improved perturbation series

Exact solution of the two-loop renormalization group equation for x with variable $t=\log(q^2/\Lambda^2)$,

$$\beta(x) = \frac{dx}{dt} = -\frac{b}{2}x^2(1+cx), \tag{12}$$

is

$$\frac{b}{2}\log(q^2/\Lambda^2) = \frac{1}{x} - c\log\left(\frac{1}{x}+c\right). \tag{13}$$

The solution x can be expressed as

$$x(q^2) = -\frac{1}{c}\frac{1}{1+W(z)},$$

where $W(z)$ is the Lambert W function which satisfies $W(z)e^{W(z)}=z$. We apply the dispersion relation and consider contributions on a cut of negative real axis in the space of q^2—i.e., take q pure imaginary. In order to be consistent with the $\overline{\rm MS}$ scheme, the variable z is defined as

$$z = -e^{(-1-bt/2c)} = -\frac{1}{e}\left(\frac{q}{\tilde{\Lambda}_{\overline{\rm MS}}}\right)^{-b/c} e^{iK\pi} = -Z(q^2)e^{iK\pi}, \tag{14}$$

where $t=\log(q^2/\tilde{\Lambda}^2_{\overline{\rm MS}})$, $\tilde{\Lambda}_{\overline{\rm MS}}=(2c/b)^{-c/b}\Lambda_{\overline{\rm MS}}$, $K=-b/2c$ [23,25]. The physical quantities $\mathcal{R}$ are expressed in a series:

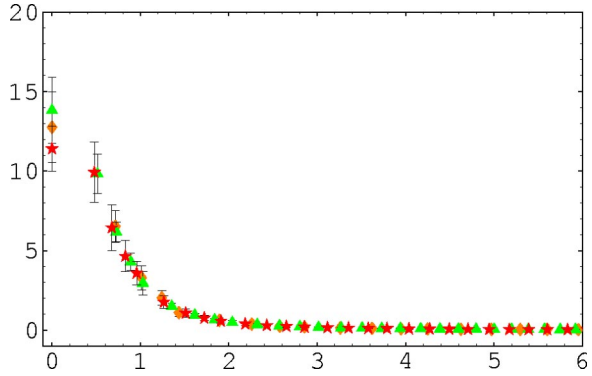

FIG. 1. The gluon propagator as a function of the momentum q (GeV). $\beta=6.0$, 24^4 (triangles), 32^4 (diamonds), and $\beta=6.4$, 48^4 (stars) in the log U definition.

$$\mathcal{R}(q^2) = \mathcal{B}_1(q^2) + \sum_{n=1}^{\infty} A_n \mathcal{B}_{n+1}(q^2), \tag{15}$$

$$\mathcal{B}_n = \frac{1}{2\pi}\int_{-\pi}^{\pi}\left(\frac{-1}{c(1+W(Z(q^2)e^{iK\theta})}\right)^n d\theta. \tag{16}$$

III. LATTICE DATA

A. Gluon propagator

The gluon propagator on the lattice was measured by using cylindrical cut method [12]—i.e., choosing momenta close to the diagonal direction. When the difference of their lattice constant $a^{-1}=1.885$ GeV in $\beta=6.0$, $32^3\times 64$ and our $a^{-1}=1.97$ GeV, 32^4 is taken into account, the data are consistent with [12] (see Fig. 1).

The effective coupling y of the $\widetilde{\rm MOM}$ scheme is calculated from

$$1/y = \beta_0 \log(\mu/\Lambda_z)^2 - \frac{\beta_1}{\beta_0}\log(\beta_0 y) \tag{17}$$

for $\mu=1.97$ GeV and $\Lambda_z=\Lambda_{\overline{\rm MS}}e^{25085/37752}$ [28] obtained from the three-gluon vertex in Landau gauge perturbation theory. The relevant solution of Eq. (17) is $y=0.02227$.

The gluon dressing function is defined as $Z_A(q^2)=q^2D_A(q^2)$. Its inverse Z^{-1} is expressed in the two-loop perturbation series as [28]

$$Z^{-1}(q^2,y) = \lambda_z^{-1}h^{(2)-13/22}\left[1-\frac{25085}{2904}h^{(2)} - \left(\frac{41245993}{1874048}-\frac{9747}{352}\zeta_3\right)h^{(2)2}\right], \tag{18}$$

where λ_z is a fitting parameter (see Fig. 3).

As shown in Fig. 1 and Fig. 3, the gluon propagators of 24^4, 32^4, and 48^4 as a function of the physical momentum agree quite well with one another and they can be fitted by

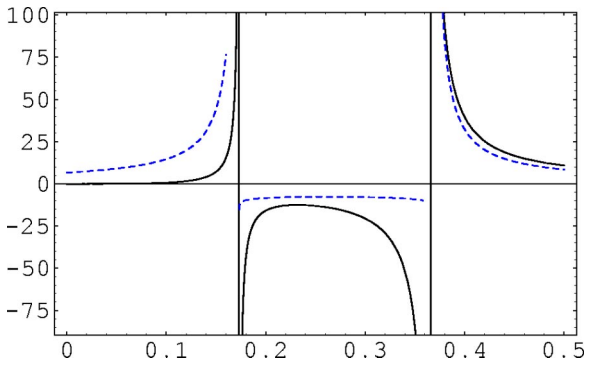

FIG. 2. The dressing function $\lambda_z Z(q^2,y)$ as a function of the variable z for a fixed $y=0.02227$. The branches of the Lambert W funtion $1/W_0(0.17-z)$, $\mathrm{Re}[W_{-1}(0.17-z)+W_{-1}(z-e^{-1})]$, and $1/W_0(z-e^{-1})$ are shown as dotted lines.

$$D_A(q^2)=\frac{Z(q^2,y)|_{y=0.02227}}{q^2}=\frac{Z_A(q^2)}{q^2} \tag{19}$$

in the $q>0.8$ GeV region. At zero momentum, $D_A(0)$ decreases as the lattice size becomes larger.

The gluon dressing function in the $\widetilde{\mathrm{MOM}}$ scheme with $y=0.02227$ fits the lattice data for $q>0.8$ GeV, but there appears a discontinuity at $z\simeq 0.174$ and $z=1/e$. We note that the q dependence of $Z(q^2,y)$ in $z<0.17$ is similar to $1/W_0(0.17-z)$, that in $0.17<z<1/e$ is similar to $\mathrm{Re}[W_{-1}(0.17-z)+W_{-1}(z-e^{-1})]$, and that in $z>1/e$ is similar to $1/W_0(z-1/e)$.

B. Ghost propagator

The ghost dressing function is defined by the ghost propagator as $G^{ab}(q^2)=q^2 D_G^{ab}(q^2)$. In the $\widetilde{\mathrm{MOM}}$ scheme, we fix the scale by choosing y as a solution of

$$1/y=\beta_0 \log(\mu/\Lambda_{gh})^2-\frac{\beta_1}{\beta_0}\log(\beta_0 y). \tag{20}$$

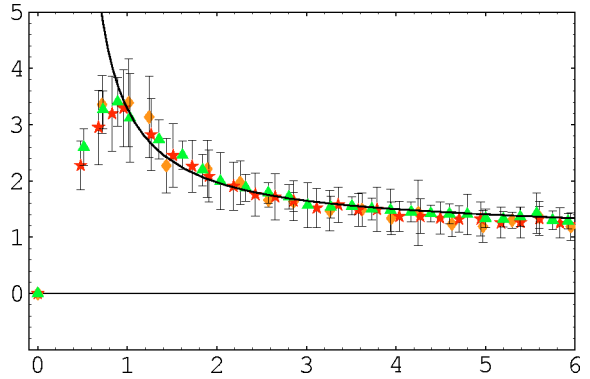

FIG. 3. The gluon dressing function as the function of the momentum q (GeV). $\beta=6.0$, 24^4 (triangles), 32^4 (diamonds), and $\beta=6.4$, 48^4 (stars) in the $\log U$ version. The fitted line is that of the $\widetilde{\mathrm{MOM}}$ scheme.

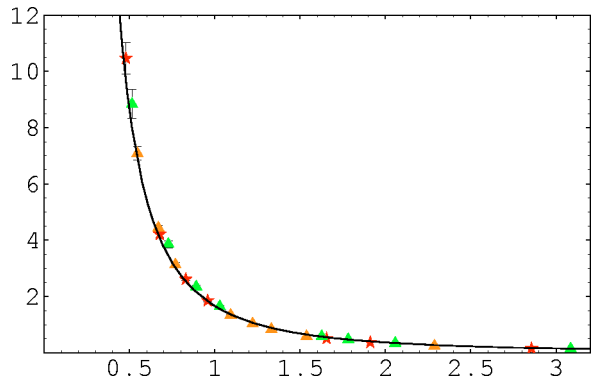

FIG. 4. The ghost propagator as the function of the momentum q (GeV). $\beta=6.0$, 24^4, 32^4 and $\beta=6.4$, 48^4 in the $\log U$ version. The fitted line is that of the $\widetilde{\mathrm{MOM}}$ scheme. $Z_g(q^2,y)$ is singular at $\tilde{\Lambda}_{\overline{\mathrm{MS}}}\simeq 0.25$ GeV which should be washed away by the nonperturbative effects.

For $\mu=1.97$ GeV and $\Lambda_{gh}=\Lambda_{\overline{\mathrm{MS}}}e^{1757/2904}$ [28] obtained from two-loop Landau gauge perturbation theory, we find as a relevant solution $y=0.02142$.

The ghost dressing function is

$$Z_g^{-1}(q^2,y)=\lambda_g^{-1}h^{(2)-9/44}\left[1+h^{(2)}\left(-\frac{5271}{1936}\right)+h^{(2)2}\left(-\frac{615512003}{7496192}+\frac{5697}{704}\zeta_3\right)+\cdots\right], \tag{21}$$

where λ_g is a fitting parameter.

In Fig. 4, the 24^4, 32^4, and 48^4 lattice data are compared with

$$D_G(q^2)=-\frac{Z_g(q^2,y)|_{y=0.02142}}{q^2}=\frac{G(q^2)}{q^2}. \tag{22}$$

We observe that the agreement is good for $q>0.5$ GeV and better than the result of the PMS method of [27]. The ghost propagators were calculated by the perturbative method and the straightforward and preconditioned CG methods. We found that the two CG methods are consistent and give better accuracy than the perturbative method in SU(2) and give correct result in the lowest-momentum point of the SU(3) 48^4 lattice. With the lowest-momentum point of the 48^4 lattice calculated with the CG method, the whole data can be fitted by Eq. (22).

C. QCD running coupling

We measured the running coupling from the product of the gluon dressing function and the ghost dressing function squared [9]:

$$\alpha_s(q^2)=\frac{g_0^2}{4\pi}Z_A(q^2)G(q^2)^2\simeq(qa)^{-2(\alpha_D+2\alpha_G)}. \tag{23}$$

The lattice size dependences of the exponents α_D and α_G are summarized in Table I.

TABLE I. The exponent of gluon dressing function near zero momentum α_D, near $qa=1$ α'_D, and the exponent of the ghost dressing function near zero momentum α_G. log U type.

β	L	α_D	α'_D	α_G	$\alpha_D+2\alpha_G$
6.0	32	−0.375	0.302	0.174	−0.03(10)
6.4	48	−0.273	0.288	0.193	0.11(10)

The effective running coupling in the $\overline{\text{MS}}$ scheme is expressed by the series of coupling constants $h^{(n)}$ as Eq. (6) [27,28]. The result of the $\widetilde{\text{MOM}}$ scheme using $y=0.01594$ is shown by the solid line in Fig. 5. The lattice data of 24^4, 32^4, and 48^4 and the $\widetilde{\text{MOM}}$ scheme agree at 0.5 GeV$<q<$2 GeV, but the fit is slightly overestimated at $q>2$ GeV.

In the contour-improved perturbation series, the running coupling in two loops is expressed as

$$\mathcal{R}^2(q^2)=\mathcal{B}_1(q^2)+A_1\mathcal{B}_2(q^2)+A_2\mathcal{B}_3(q^2)+\cdots. \quad (24)$$

The series truncated at order A_1 is plotted in Fig. 6 together with the 48^4 lattice data measured by using the log$U$ definition. We observed that the fit is good for $q>2$ GeV, but the nonperturbative effect is underestimated.

Since in the perturbative calculation of the Landau gauge gluon vertex in the $\overline{\text{MS}}$ scheme the $\Lambda_{\overline{\text{MS}}}$ is modified to $e^{70/6\beta_0}\Lambda_{\overline{\text{MS}}}$ [30], we performed the same replacement. The result is overestimated in the $q>1$ GeV region. Since the A_3 term is not known and there are cancellations between successive terms, we fit the data by inclusion of half of the A_2 term. The result is shown by the dotted line in Fig. 6.

The similar nonperturbative effect was attributed to the gluon condensates in [11,31]. The lattice data are qualitatively the same as the results of hypothetical τ lepton decay [32], and the Dyson-Schwinger approach [33].

The lowest-momentum point of α_s of $\beta=6.4$, 48^4 becomes consistent with results of other lattice sizes when it is calculated with the CG method.

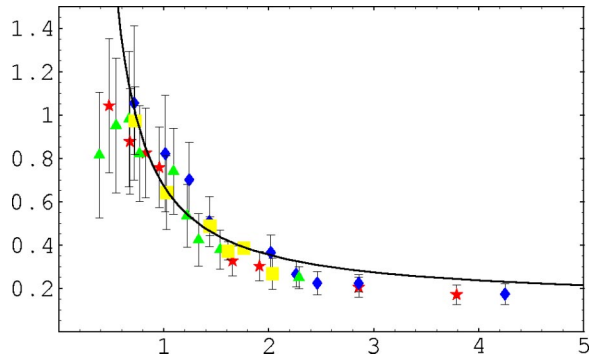

FIG. 5. The running coupling $\alpha_s(q)$ of $\beta=6.0$, 24^4 (squares), 32^4 (triangles), $\beta=6.4$, 32^4 (diamonds), and 48^4 (stars) as a function of momentum q (GeV) and the result of the PMS method in the $\widetilde{\text{MOM}}$ scheme.

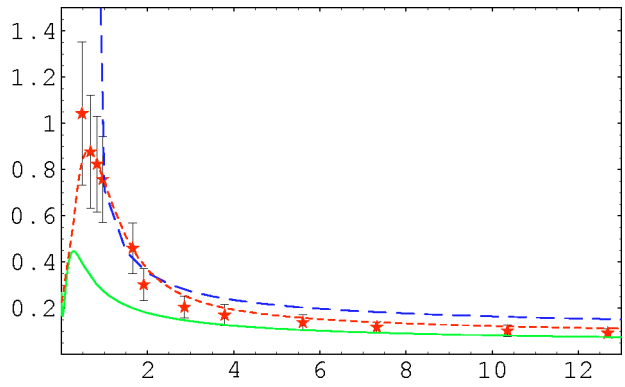

FIG. 6. The running coupling $\alpha_s(q)$ as a function of momentum q (GeV) of the $\beta=6.4$, 48^4 lattice. The solid line is the result of $\mathcal{R}^2$ using $\Lambda_{\overline{\text{MS}}}=237$ MeV. The dotted line is the result of $e^{70/6\beta_0}\tilde{\Lambda}_{\overline{\text{MS}}}$ and including half of A_2. The dashed line is the result of the $\widetilde{\text{MOM}}$ scheme.

D. Kugo-Ojima parameter

Our lattice data of (1) The Kugo-Ojima parameter $c=-u(0)$, (2) the trace of the gauge field divided by the dimension e/d, and (3) the deviation parameter h from the horizon condition [13] are summarized in Table II.

We observe that the Kugo-Ojima parameter of the U-linear definition remains smaller than that of log U. The similar difference exists in the ghost propagator in the infrared region.

We plot in Fig. 7, the value c as a function of log $Z(\mu^2)$ of $\beta=6.0$, 16^4, and 24^4 in log U and U-linear definitions and $\beta=6.4$, 32^4, and 48^4 in the log U definition. The value c of $\beta=6.0$, 32^4 is almost the same as 24^4. The value increases as the lattice size increases from 16^4 to 24^4 and the extrapolation of the two definitions to those of a large lattice where c in log U and U-linear seem to cross at $c\sim1$. The linear extrapolation as the function of log $Z(\mu^2)$ is based on the factorizability

$$Z_3(\mu^2,\Lambda_{\widetilde{MOM}})=Z_R(\mu^2)/Z_b(\Lambda_{\widetilde{MOM}}) \quad (25)$$

when $\mu\sim1.97$ GeV, which allows us to express

$$Z_3(\mu^2,\Lambda_{\widetilde{MOM}})=Z_3(\mu^2,\Lambda_{\overline{\text{MS}}})\times[Z_b^{-1}(\Lambda_{\widetilde{MOM}})/Z_b^{-1}(\Lambda_{\overline{\text{MS}}})]. \quad (26)$$

The difference of the speed of $Z_b(\Lambda_{\widetilde{MOM}})$ to its continuum limit in the U-linear and log U definitions will appear as a

TABLE II. The Kugo-Ojima parameter c in the U-linear and log U versions. $\beta=6.0$ and 6.4.

β	L	c_1	e_1/d	h_1	c_2	e_2/d	h_2
6.0	16	0.576(79)	0.860(1)	−0.28	0.628(94)	0.943(1)	−0.32
6.0	24	0.695(63)	0.861(1)	−0.17	0.774(76)	0.944(1)	−0.17
6.0	32	0.706(39)	0.862(1)	−0.15	0.777(46)	0.944(1)	−0.16
6.4	32	0.650(39)	0.883(1)	−0.23	0.700(42)	0.953(1)	−0.25
6.4	48				0.793(61)	0.954(1)	−0.16

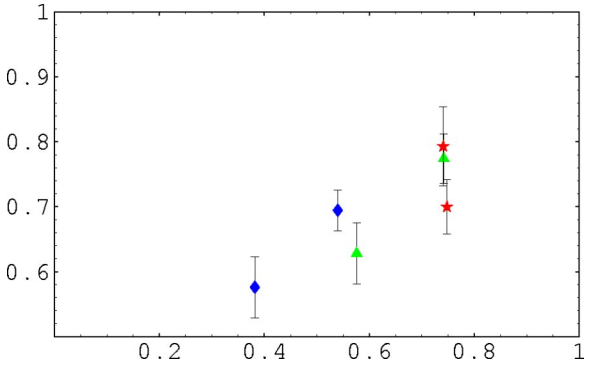

FIG. 7. The Kugo-Ojima parameter c as a function of $\log Z(1.97\ \mathrm{GeV})$. $\beta=6.4$, 32^4, 48^4 in $\log U$ (star), $\beta=6.0$, 16^4, and 24^4 in $\log U$ (triangles) and U-linear (diamonds) versions.

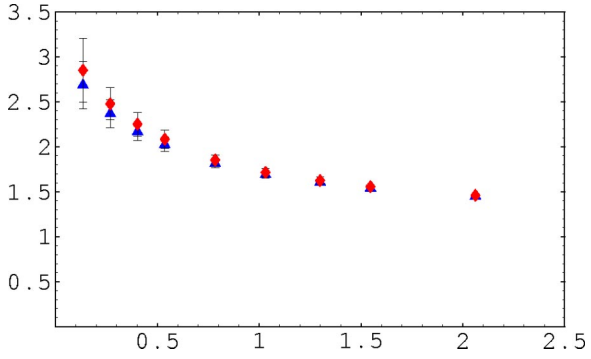

FIG. 9. The color diagonal ghost dressing function $D_G(q^2)\times q^2$ as a function of the momentum squared q^2 (GeV^2). The first copies (diamonds) are more singular than PT (triangles).

difference of the slope. However, the increase of c from 24^4 to 32^4 is small. The Kugo-Ojima parameter c of $\beta=6.4$, 48^4 lattice calculated in the CG method is 0.793(61), which is consistent to the result of the $\log U$ definition of $\beta=6.0$, 24^4, and 32^4 lattice data.

IV. SU(2) LATTICE DATA

In the numerical simulation of the SU(2) Yang-Mills field, we took the U-linear-type gauge field and simulated $\beta=2.2$ and 16^4 lattices. We took 67 samples taken after 18 000 thermalization sweeps and up to 84 000 sweeps with intervals of 1000 sweeps [16]. To each sample, we performed parallel tempering gauge fixing (PT) and direct gauge fixing by the overrelaxation method (first copy). We define the scale by the relation $1/a=0.938$ GeV and compare our data with those of [34,35] and [47].

A. Gluon propagator

The gluon propagator is shown in Fig. 8. We observe that above 1 GeV our data agree with [34], but in the infrared region our data have an enhancement. Suppression at 0 momentum is consistent with the data of [35].

B. Ghost propagator

The color diagonal component of the ghost propagator calculated in PT is about 6% less singular than that of first copy (Fig. 9). We performed the calculation of the FP inverse operator by using the CG method, since the matrix is symmetric positive definite. Our data in the infrared are less singular than that of [34]. Although there are differences in the gauge fixing method (PT versus simulated annealing), we do not understand the origin of the difference.

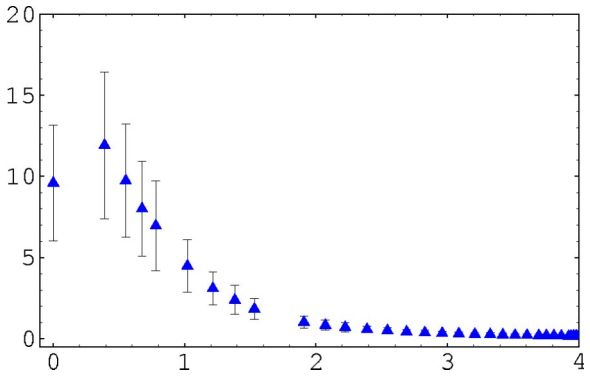

FIG. 8. The gluon propagator $D_A(q)$ as a function of the momentum q (GeV) of PT samples.

In the maximal Abelian (MA) gauge, color symmetry is spontaneously broken by the ghost condensation [36,37]. In the Landau gauge, there is no background field as in the MA gauge, but the structure of the color off-diagonal ghost propagator has not been known. In order to investigate this problem, we measured color off-diagonal symmetric and antisymmetric $[\epsilon_{abc}D_G^{ab}(q,q)]$ matrix elements, where $D_G^{ab}(q,q)$ is the ghost propagator with color indices a and b. We observed that the color off-diagonal antisymmetric part is consistent with zero pointwise as is expected from the theoretical observation and that the color off-diagonal symmetric part multiplied by q^4 is consistent with zero over the ensemble average, but its standard deviation is almost constant in the whole momentum region. The fluctuation can be parametrized as σ/q^4 with $\sigma=0.0176(28)$ GeV^2, in the normalization tr $\tau^2=1$. We observed the same qualitative features in the SU(3) 48^4 lattice, but σ is about 1/9 of the SU(2) 16^4 lattice, i.e., the fluctuation is statistical.

C. QCD running coupling

The result of the running is shown in Fig. 10. As a result of the difference in the ghost propagator, the running coupling is about 1/3 of [34]. We observe suppression near 0 momentum.

D. Kugo-Ojima parameter

The Kugo-Ojima parameter c of the PT samples was 0.690(52) and that of the first copy was 0.722(68). This difference is qualitatively the same as that of the ghost dressing function at 0 momentum.

V. CONCLUSION AND OUTLOOK

There are two aspects of color confinement: i.e., (1) the presence of long-range correlation between colored sources and (2) the absence of massless gluon poles. The Kugo-

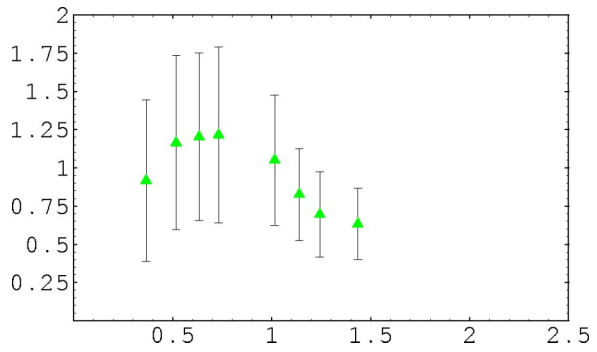

FIG. 10. The running coupling $\alpha_s(q)$ as a function of the momentum q (GeV) of PT samples.

Ojima criterion is a sufficient condition for the two aspects, but the lattice data do not verify that these criteria are satisfied.

A new method of FMR gauge fixing in SU(2) is reported in [16]. We observe that the gluon propagator is suppressed at zero momentum in SU(2)—i.e., the exponent $\alpha_D < -0.5$—in contrast to the SU(3) case where $\alpha_D \geqslant -0.5$. In the simulation of SU(2), we observed differences in the Kugo-Ojima parameter of the configuration in the FMR and of copies randomly produced in the Gribov region. The Gribov copy affects the Kugo-Ojima parameter, and in the ghost propagator in the infrared region, the difference is about 4%. Color SU(3) contains I, U, and V SU(2) spin components, and we expect that the Gribov ambiguity is the same order.

In the lattice data, the singularity of the ghost propagator is stronger than the tree level and that of the gluon propagator is weaker than the tree level. The dependence on the U-linear or $\log U$ definition of the gauge field is small in the gluon propagator, consistent with [38], but not negligible in the FP inverse operator.

We aimed at detecting in the lattice dynamics a signal of the Kugo-Ojima confinement criterion derived in the continuum theory, formulated with use of the FP Lagrangian and BRST symmetry. We also noted that Zwanziger's horizon condition, based on the lattice formulation, coincides with the Kugo-Ojima criterion [3,13]. However, our present data are not satisfactory to prove or disprove the confinement criterion. The color off-diagonal antisymmetric part of the ghost propagator [36,39] vanishes in the Landau gauge, but the off-diagonal symmetric part has fluctuations proportional to $(qa)^{-4}$.

Although there are problems in fixing y of the PMS in the low-energy region, an extension of the effective charge method is a possible solution. In an extension of the solution of the two-loop renormalization group equation expressed by the Lambert W function, a solution of Padé approximant of the three-loop renormalization group equation was shown [40] and numerical calculation was done for $N_f \geqslant 3$ [41]. In the analytical perturbation theory approach in one loop, one predicts [42] a nonperturbative infrared fixed point of

$$\frac{\alpha_s(0)}{4\pi} = \frac{1}{\beta_0} = \frac{1}{11-2/3N_f}.$$

Extension to two loops is discussed in [40]. For $N_f=0$, one needs continuation. There is a conjecture, in combination with the conformal relation, that continuation from N_f in the conformal window ($4 \leqslant N_f \leqslant 6$) to $N_f=0$ would be possible [29,43,44].

We remark that the Orsay group analyzed QCD running coupling in the Landau gauge from a three-gluon vertex. They separate the momentum space into $q<0.8$ GeV and 1.5 GeV$<q$ and fit the lower-momentum region by the instanton liquid model and the higher-momentum region by including the $1/q^2$ power correction due to gluon condensates [45]. We did not take $\alpha_s(0)=0$. Agreement of the lattice results of QCD running coupling in $q>0.8$ GeV region and the 3 loop perturbation theory is reported in [46].

We observed that the contour-improved perturbation theory performs a resummation of the perturbation series and that we can understand qualitatively the Landau gauge lattice QCD data via these methods.

ACKNOWLEDGMENTS

We are grateful to Daniel Zwanziger for enlightening discussions. S.F. thanks Kei-Ichi Kondo, Stanley Brodsky, Karel van Acoleyen, David Dudal, and Kurt Langfeld for valuable information. This work is supported by the KEK supercomputing project No. 03-94.

APPENDIX: THE NUMERICAL CALCULATION OF THE FADDEEV-POPOV INVERSE

In this appendix we briefly explain the numerical method of calculating the Faddeev-Popov inverse.

1. Perturbative method

The ghost propagator, which is the Fourier transform of an expectation value of the inverse Faddeev-Popov operator $\mathcal{M} = -\partial D = -\partial^2(I-M)$,

$$D_G^{ab}(x,y) = \langle \mathrm{tr} \langle \lambda^a x | (\mathcal{M}[U])^{-1} | \lambda^b y \rangle \rangle, \qquad \text{(A1)}$$

where the outmost $\langle \cdots \rangle$ denotes average over samples U, is evaluated as follows. We take the plane wave for the source $\mathbf{b}^{[1]} = \boldsymbol{\lambda}^b e^{iqx}$ and get the solution $-\Delta \boldsymbol{\phi}^{[1]} = \mathbf{b}^{[1]}$. Here $\boldsymbol{\phi}^{[1]} = (-\Delta)^{-1}\mathbf{b}^{[1]}$. We calculate iteratively $\phi^{[i+1]} = M\boldsymbol{\phi}^{[i]}(\mathbf{x})$ $(i=1,\ldots,k-1)$. The iteration was continued until the maximum norm $\mathrm{Max}_{\mathbf{x}}|\boldsymbol{\phi}^{[k]}(\mathbf{x})|/\mathrm{Max}_{\mathbf{x}}|\Sigma_{i=1}^{k-1}\boldsymbol{\phi}^{[i]}(\mathbf{x})| < 0.001$–$0.01$. The number of iterations k, is of the order of 60, in SU(2), 16^4 lattice, and of the order of 100 in SU(3). We measure also the ℓ_2 norm $\|\boldsymbol{\phi}^{[k]}(\mathbf{x})\|/\|\Sigma_{i=1}^{k-1}\boldsymbol{\phi}^{[i]}(\mathbf{x})\|$.

We define $\boldsymbol{\Phi}^b(\mathbf{x}) = \Sigma_{i=1}^{k}\boldsymbol{\phi}^{[i]}(\mathbf{x})$ and evaluate $\langle \lambda^a e^{iqx}, \Phi^b(\mathbf{x}) \rangle$ as the ghost propagator from color b to color a.

In the low-momentum region of SU(2) we observed a specific color symmetry violation pattern, and in the case of SU(3) relatively large color off-diagonal matrix elements suppressed the color diagonal matrix element. For a cross-check of the perturbative method, we adopted the straightfor-

ward conjugate gradient method and the preconditioned conjugate gradient method [22] in which the truncated perturbation series is used for the preconditioning.

2. Preconditioned conjugate gradient method

We define $\mathcal{M}=-\partial^2(I-M)$ and define the truncated $\mathcal{M}^{-1}$ which is used in the perturbative method as $B^{-1}=(I+M+\cdots+M^{m-1})(-\Delta)^{-1}$. First we choose $\mathbf{x}^0$ and define $\mathbf{r}^0=\mathbf{b}-\mathcal{M}\mathbf{x}^0$. Using the multigrid Poisson solver we calculate the perturbation series

$$\tilde{\mathbf{r}}^0=B^{-1}\mathbf{r}^0 \tag{A2}$$

and define $\mathbf{p}^0=\tilde{\mathbf{r}}^0$.

Then we begin the iteration for $k=0,1,\ldots,$

$$\alpha_k=-(\tilde{\mathbf{r}}^k,\mathbf{r}^k)/(\mathbf{p}^k,\mathcal{M}\mathbf{p}^k), \tag{A3}$$

$$\mathbf{x}^{k+1}=\mathbf{x}^k-\alpha_k\mathbf{p}^k, \tag{A4}$$

$$\mathbf{r}^{k+1}=\mathbf{r}^k+\alpha_k\mathcal{M}\mathbf{p}^k. \tag{A5}$$

We check the norm of $\mathbf{r}^{k+1}$, and if it is not small, we calculate the perturbation series $\tilde{\mathbf{r}}^{k+1}=B^{-1}\mathbf{r}^{k+1}$ as before. We define

$$\beta_k=(\tilde{\mathbf{r}}^{k+1},\mathbf{r}^{k+1})/(\tilde{\mathbf{r}}^k,\mathbf{r}^k), \tag{A6}$$

$$\mathbf{p}^{k+1}=\tilde{\mathbf{r}}^{k+1}+\beta_k\mathbf{p}^k, \tag{A7}$$

and go back to the beginning of the iteration cycle. By choosing a sufficiently large number of m, the convergence occurs after a few iteration cycles.

The preconditioned method makes the l_2 norm convergence faster than the straightforward conjugate gradient method, but its maximum norm is larger than that of straightforward method. The solution agrees with the straightforward conjugate gradient method within errors in the whole momentum region, but disagrees with the perturbative method in the lowest-momentum point of $\beta=6.4$, SU(3) 48^4 lattice [47].

[1] T. Kugo and I. Ojima, Prog. Theor. Phys. Suppl. **66**, 1 (1979).
[2] V.N. Gribov, Nucl. Phys. **B139**, 1 (1978).
[3] D. Zwanziger, Nucl. Phys. **B364**, 127 (1991); **B412**, 657 (1994).
[4] D. Zwanziger, Phys. Rev. D **69**, 016002 (2004).
[5] J.E. Hetrick and P.H. de Forcrand, Nucl. Phys. B (Proc. Suppl.) **63A-C**, 838 (1999).
[6] K.I. Kondo, hep-th/0303251.
[7] F.D.R. Bonnet *et al.*, Phys. Rev. D **64**, 034501 (2001).
[8] M. Chaichian and K. Nishijima, hep-th/9909159 and references therein.
[9] L. von Smekal, A. Hauck, and R. Alkofer, Ann. Phys. (N.Y.) **267**, 1 (1998).
[10] A. Cucchieri and D. Zwanziger, Phys. Lett. B **524**, 123 (2002).
[11] D. Becirevic *et al.*, Phys. Rev. D **61**, 114508 (2000).
[12] D.B. Leinweber, J.I. Skullerud, A.G. Williams, and C. Parrinello, Phys. Rev. D **60**, 094507 (1999); **61**, 079901 (2000).
[13] H. Nakajima and S. Furui, Nucl. Phys. B (Proc. Suppl.) **63A-C**, 635 (1999); **63A-C**, 865 (1999); **83-84**, 521 (2000); **119**, 730 (2003); Nucl. Phys. **A680**, 151c (2000); hep-lat/0007001; Nucl. Phys. B (Proc. Suppl.) **119**, 730 (2003).
[14] S. Furui and H. Nakajima, in *Quark Confinement and the Hadron Spetrum IV*, edited by W. Lucha and K.M. Maung (World Scientific, Singapore, 2002, p. 275), hep-lat/0012017.
[15] H. Nakajima and S. Furui, in *Strong Coupling Gauge Theories and Effective Field Theories*, edited by M. Harada, Y. Kikukawa, and K. Yamawaki (World Scientific, Singapore, 2003, p. 67), hep-lat/0303024.
[16] H. Nakajima and S. Furui, in Lattice '03 proceedings 2003, hep-lat/0309165.
[17] N. Cabibbo and E. Marinari, Phys. Lett. **119B**, 387 (1982).
[18] A.D. Kennedy and B.J. Pendleton, Phys. Lett. **156B**, 393 (1985).
[19] T. Maskawa and H. Nakajima, Prog. Theor. Phys. (Kyoto) **60B**, 1526 (1978); **63**, 641 (1980).
[20] M.A. Semenov-Tyan-Shanskii and V.A. Franke, Zap. Nauchn. Semin. LOMI **120**, 159 (1982).
[21] W. Hackbusch, *Multi-Grid Methods and Applications*, Springer Series in Computational Mathematics Vol. 4 (Springer, Berlin, 1980).
[22] J.M. Orthega, *Introduction to Parallel and Vector Solution of Linear Systems* (Plenum, New York, 1988), p. 200.
[23] P.M. Stevenson, Phys. Rev. D **23**, 2916 (1981).
[24] G. Grunberg, Phys. Rev. D **29**, 2315 (1984).
[25] D.M. Howe and C.J. Maxwell, Phys. Lett. B **541**, 129 (2002).
[26] G.'t Hooft, in *The Whys of Subnuclear Physics*, edited by A. Zichichi (Plenum, New York, 1978), pp. 943–971.
[27] K. van Acoleyen and H. Verschelde, Phys. Rev. D **66**, 125012 (2002).
[28] K.G. Chetyrkin and A. Retey, hep-ph/0007088.
[29] S.J. Brodsky and H.J. Lu, Phys. Rev. D **51**, 3652 (1995).
[30] W. Celmaster and R.J. Gonsalves, Phys. Rev. D **20**, 1420 (1979).
[31] Ph. Boucaud *et al.*, J. High Energy Phys. **04**, 006 (2000).
[32] S.J. Brodsky, S. Menke, and C. Merino, Phys. Rev. D **67**, 055008 (2003).
[33] C.S. Fischer, R. Alkofer, and H. Reinhardt, Phys. Rev. D **65**, 094008 (2002).
[34] J.R.C. Bloch, A. Cucchieri, K. Langfeld, and T. Mendes, Nucl. Phys. B (Proc. Suppl.) **119**, 736 (2003).
[35] C. Alexandrau, Ph. de Forcrand, and E. Follena, hep-lat/0009003.
[36] K-I. Kondo and T. Shinohara, Phys. Lett. B **491**, 263 (2000).
[37] M. Shaden, in *Quark Confinement and Hadron Spectrum VI*, edited by W. Lucha and K.M. Maung (World Scientific, Singapore, 2002), p. 258.
[38] I.L. Bogolubovsky and V.K. Mitrjushkin, hep-lat/0204006.
[39] D. Dudal, H. Vershelde, V.E.R. Lemes, M.S. Sarandy, S.P.

Sorella, M. Picariello, A. Vicini, and J.A. Gracey, J. High Energy Phys. **06**, 003 (2003).
[40] E. Gardi, G. Grunberg, and M. Karliner, J. High Energy Phys. **07**, 007 (1998).
[41] B.A. Magradze, hep-ph/0010070.
[42] D.V. Shirkov, Teor. Mat. Fiz. **136**, 3 (2003) [Theor. Math. Phys. **136**, 893 (2003)], and references therein.
[43] S.J. Brodsky, E. Gardi, G. Grunberg, and J. Rathsman, Phys. Rev. D **63**, 094017 (2001).
[44] G. Grunberg, Phys. Rev. D **65**, 021701(R) (2001).
[45] Ph. Boucaud *et al.*, Phys. Rev. D **63**, 114003 (2001); J. High Energy Phys. **04**, 005 (2003).
[46] M. Lüscher, in *International Conference on Theoretical Physics, TH2002*, edited by D. Iagolnitzer *et al.* (Birkhäuser, Basel, 2003), pp. 197–210; hep-ph/0211220.
[47] A. Cucchieri, Nucl. Phys. **B508**, 353 (1997).